A MONTE CARLO CORRECTION FOR COMPTON SCATTERING EFFECTS IN 3D PET BRAIN IMAGING

C.S. Levin, M. Dahlbom, E.J. Hoffman
UCLA School of Medicine Division of Nuclear Medicine and Biophysics
Los Angeles, CA 90024

Abstract

A Monte Carlo simulation has been developed to simulate and correct for Compton scattering effects in 3D acquired PET brain images. As input the routine requires the 3D reconstructed image volume of interest which is treated as a source intensity distribution for a photon-tracking Monte Carlo simulation. It is assumed that the number of counts in each pixel of the image represents the number of back-to-back 511 keV photon pairs being emitted at that location in the brain. The program then follows the history of each photons' interactions in the scattering medium and generates the sinograms for the scattered and unscattered photon pairs detected in a simulated 3D PET acquisition. The calculated scatter contribution is then subtracted from the original data set. The calculation is general and can be applied to any scanner configuration or geometry. In its current form the simulation requires 25 hours on a single Sparc10 CPU when every pixel in a 15-plane, 128x128 pixel image volume is studied, and less than 2 hours when sampled over regions of 4x4 pixels. Results of the correction applied to 3D human and phantom studies are presented.

I. INTRODUCTION

In order to realize the full potential of spatial resolution improvements that the current positron emission tomography (PET) system detector designs offer, the sensitivity must be improved [1]. Large sensitivity increases (a factor of 5-7) are realized when the inter-plane septa are removed and all possible lines of response acquired [2, 3]. Unfortunately, this three-dimensional (3D) mode of acquisition results in a large (3-fold) increase in scatter fraction compared to the conventional two-dimensional mode with septa. This increase in background events prevents accurate quantitation and degrades image contrast. The development of an accurate and efficient scatter correction is essential before 3D acquired PET can be routinely employed across a wider spectrum of imaging conditions.

Currently, there are a number of promising approaches to scatter correction for 3D PET [3-10]. Most of these methods, however, rely on certain empirical information that is assumed to be valid independent of source distribution and attenuating media. In reality the scatter distributions for realistic sources and scattering media have a complex dependency on the source distribution and the object composition and shape. Any generalizations or simplifying assumptions cannot be expected to hold for all situations and are bound to compromise accuracy. In addition, those methods that require supplementary measurements produce additional noise and may require longer patient scanning time and/or larger data sets.

The dual energy method [4] assumes that the spatial distribution of the Compton scattered events present in measured photo-peak window data is approximately the same as that in a second, lower energy region of interest. This method requires doubling an already large 3D acquired data set. The Convolution/subtraction approach [3, 5, 6] assumes that the Compton scatter distribution is an empirically determined integral transformation of the 3D emission data. This scatter kernel is usually derived from phantom measurements, assuming that one size and shape is adequate. The 2D-3D difference method [7] relies on the smoothness of the scatter distribution and uses an additional 2D scan to estimate scatter in the oblique planes using the direct plane data. The interpolation technique [8] assumes scatter follows a certain shape function, which is fitted to the tails of profiles outside the object. The success of the fits depends on the symmetry of the activity distributions and on the presence of tails with adequate statistics. Analytic techniques [9,10] directly calculate the scatter using the emission and/or transmission data. These methods rely on certain approximations, such as, ignoring multiple scattering, assuming only one photon scatters per annihilation pair, etc. to reduce computation time.

As a preliminary effort to correct for Compton scattering effects in 3D acquired whole-body PET imaging, a Monte Carlo simulation has been developed to simulate and remove such effects in 3D PET brain imaging [11]. This method models the statistical process of photon emission and simulates the scatter distribution for complex activity and density distributions using only the 3D reconstructed image volume of interest, the detector gantry geometry and the physics of photon interactions. No assumptions are made of the shapes of the source distributions or attenuation media. However, the large computation burden may necessitate the use of parallel computing to make this approach feasible for routine clinical use. Execution time can also be reduced without parallel computing by using suitable coarse sampling rates through the input image with little loss in accuracy. The goal of this paper is to demonstrate the ability of the Monte Carlo simulation to accurately model and correct for Compton scatter effects in complex 3D activity distributions and attenuating media. Suggestions for further improvements and future prospects will also be presented.

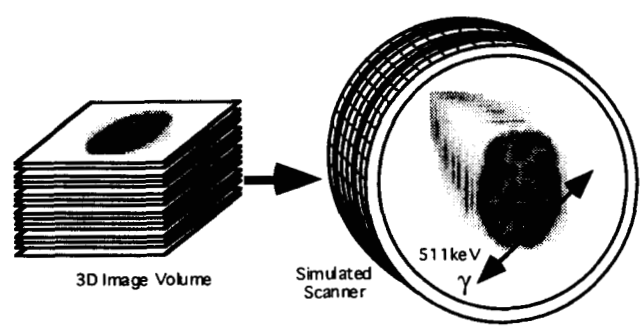

Fig. 1. Depiction of the concept of using the stacked planes of the 3D image volume as the input source distribution for a simulated 3D PET acquisition to calculate the scatter distribution.

0-7803-2544-3/95 $4.00 © 1995 IEEE

II. METHODS

This Monte Carlo scatter correction is isotope distribution dependent. The simulation requires as input the 3D acquired and reconstructed image volume that is to be corrected for Compton scattering effects. This image might include some sort of "rough" scatter correction for improved quantitation. Corrections for normalization, attenuation, randoms and dead-time are assumed to be accurate. The concept for the program input is depicted in Figure 1. The input image volume is treated as a three-dimensional source intensity distribution for a photon-tracking simulation; it is assumed that the number of counts in each pixel of the image represents the number of back-to-back 511 keV photons being emitted at that pixel location. The image volume planes are stacked and placed in the simulated scanner, assuming a common axis. The geometry of the detector gantry is determined by the number and size of individual detector crystals, including spaces between them. The program then follows the history of each photon and its interactions (Compton scattering, photo-absorption) in the scatter medium and traces escaping photons into the detector gantry in a simulated 3D acquisition. The distributions of the unscattered (primary) and total (scattered + primary) photon pairs are calculated and sorted into their respective sinograms.

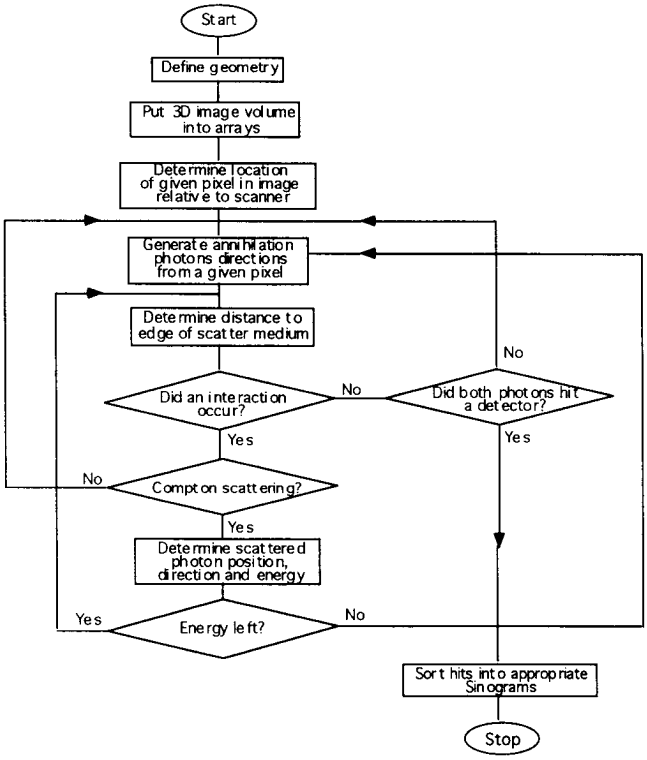

Fig. 2. Flow chart for the Monte Carlo calculation of Compton Scatter in 3D PET.

The flow chart for the simulation is shown in Figure 2. Three assumptions are made: (1) a photon is assumed to be detected where it strikes a detector surface (provided its energy is above a certain threshold), (2) the scatter effects from activity outside the field of view are negligible, and (3) the linear attenuation coefficient for the head is uniform and that of water. Multiple Compton scattering is allowed. The decision whether or not a given photon scatters is determined by both the linear attenuation coefficients of the medium and the distance from the photons' origin to the edge of the scattering medium along the line of propagation. The edge of a human brain in that direction is defined by when the pixel value of the input image activity drops below a certain threshold. For phantoms, the edge calculation depends on their geometrical shape. The determination of the energy of a scattered photon is based on the Klein-Nishina cross-section. If the photon escapes the scattering medium and hits a detector in the gantry, the event is recorded in the appropriate sinogram as either a scattered or primary event depending on its energy. The calculation is general and can be applied to any scanner configuration or geometry.

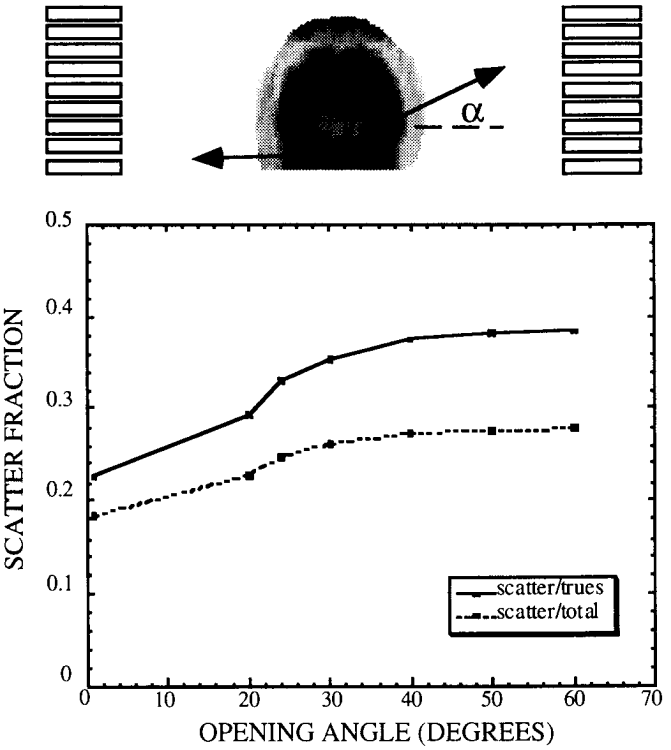

Fig. 3. Top: schematic representation of a coronal cross-section through the simulated 3D PET scanner showing the opening angle α of one of the photons from a pixel in the input image volume. Bottom: calculated scatter fraction vs. α for a simulated 3D human brain scan (trues = unscattered, total = trues + scattered).

III. RESULTS

A. Opening Angle Dependence of the Scatter

The Monte Carlo scatter calculation has been tested using 3D acquired brain images from the CTI 831 NeuroECAT system with septa retracted. The image volumes studied have 15 planes, each 128 x 128 pixels in size. Each pixel is 1.75 mm and the axial separation between planes is 6.75 mm. Since this detector gantry has only a 14% geometrical efficiency for detecting centrally emitted photons, the simulated sinograms have much lower statistics than the input image volume. The photon angular aperture in the simulation

can be lowered from 180° to somewhat compensate for this effect. Figure 3 shows a schematic representation in coronal cross-section of two photons being emitted in the scanner for a simulated 3D acquisition and how the calculated scatter fraction varies with the opening angle α of the first photon. For opening angles greater than 40° the scatter fraction in a human brain leveled off at approximately 38%. The energy threshold was set at 250 keV for these simulations.

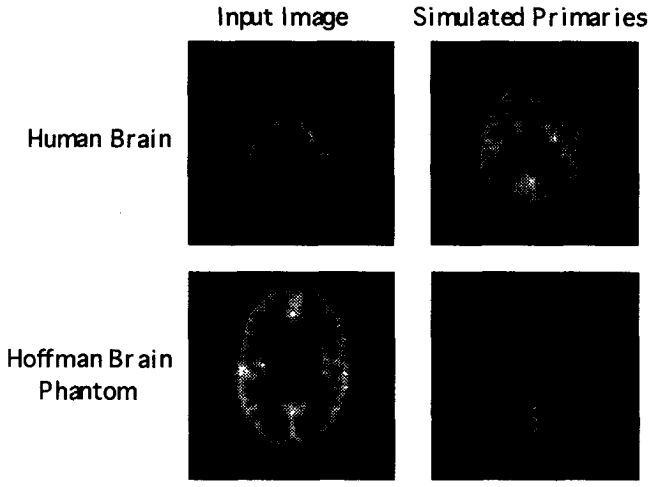

Fig. 4. A comparison between the 3D image volume input to and the reconstructed emission data generated by the simulation. The difference in noise level between the input and the calculated data is due to the geometric inefficiency of the simulated scanner.

B. Accuracy of the Modeling

Figure 4 displays a comparison between one typical plane from the input image volume and the corresponding Monte Carlo data generated from a simulated 3D PET acquisition. On the left are image planes from two 3D acquired [2] and reconstructed [12] data sets to be corrected for scatter and, on the right, the corresponding planes from the Monte Carlo generated primary photon pairs. A calculated attenuation correction was performed on the simulated primaries' sinograms [13] and the reconstruction was performed in 2D using a ramp filter at the Nyquist frequency to retain the high frequency information. The simulated images correspond well with the input to the Monte Carlo indicating that the geometry and physics are sufficiently well modeled in the routine to visually recreate the input. The difference in noise levels is due to the geometrical inefficiency of the simulated detector gantry as discussed in Section A. For the human brain image shown, the input has nearly 32 million counts while the simulated image has roughly 9 million.

C. Subtraction of the Scattered Component

Because of the lower statistics in the Monte Carlo generated data sets as compared to the input (see Fig. 4), they alone are insufficient for scatter-correction. The true 3D scatter-correction would begin by adjusting the calculated scatter-only sinogram (total - primaries) to the statistics of the input data set. This is accomplished by obtaining the scale factor between the input and Monte Carlo generated data sets: $sf = I / t$, where I and t are the gaussian-smoothed original and calculated total emission sinograms, respectively. To determine the scale-adjusted scatter component, this smooth scale factor is then multiplied by the Monte Carlo simulated scatter sinogram and the entire result again smoothed. This entire process effectively adjusts the statistics of the simulated data as shown in Fig. 4 to that of the input, while minimizing propagation of error and preserving accuracy in the result.

The scatter correction is obtained by subtracting this smooth scatter contribution from the original data set. After the scatter is removed, the original 3D acquired data set is corrected for normalization and attenuation and then 3D reconstructed using a version of the PROMIS algorithm [12]. Figure 5a displays four image planes from the un-corrected and scatter corrected 3D Hoffman Brain Phantom. No preliminary scatter correction was applied to the input image data. The corrected images have reduced statistics but better overall contrast than the uncorrected original images. Figure 5b shows profiles (2-point gaussian smoothed) through a sinogram of the original emission data without and with the Monte Carlo calculated corrections. Note how the scatter-corrected profile drops to zero at the edge of the phantom.

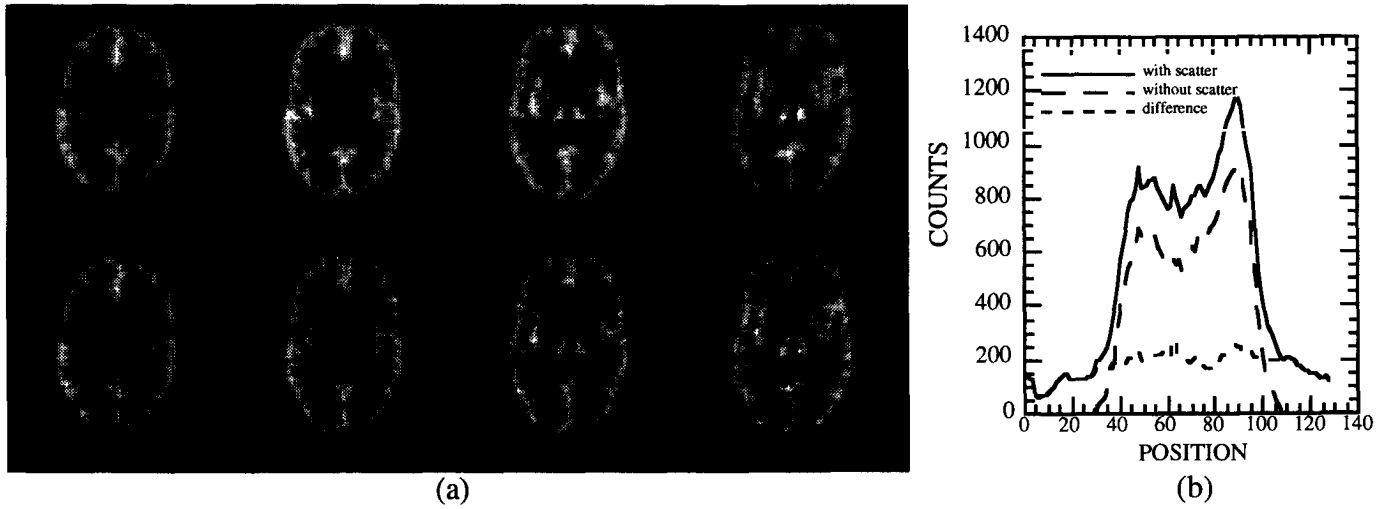

Fig. 5. (a) top row: uncorrected 3D image volume (Hoffman Brain Phantom); bottom row: with Monte Carlo scatter correction. (b) a profile through one angle of the 3D un-corrected and Monte Carlo corrected sinograms of the second plane shown in (a).

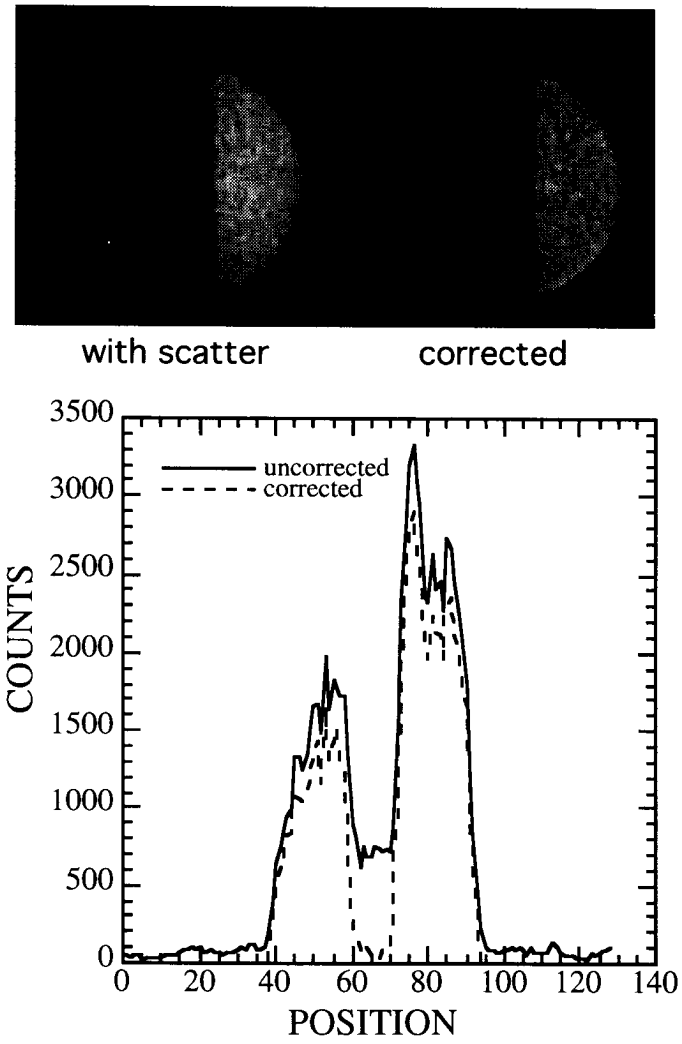

Fig. 6. Above: one plane from the un-corrected and scatter-corrected 3D Slot Phantom image volume; and below: profile through one angle of the corresponding sinogram.

To obtain a more quantitative idea of how well the calculation is removing scatter we show in Figure 6 the correction applied to the 3D acquired and reconstructed Slot Phantom. In this figure the 3D reconstructed images and smoothed profiles through a typical sinogram (corrected for attenuation) are shown. Within the slot the only activity that is measured is due to scatter. The Monte Carlo calculated correction successfully brings the activity to zero outside the object. The overall activity in the slot has been reduced to less than 2% of its original value before scatter correction. Any residual activity in the slot after the correction is most likely due to scatter activity and/or artifacts present in the input image data. A remedy for this situation is to use an iterative procedure where each time the Monte Carlo correction would be applied to the previously corrected image volume until the residual scatter is reduced to an acceptable level.

D. The Computation Time

The input image volumes discussed so far were sampled pixel by pixel in the Monte Carlo simulation. Using this high degree of sampling the total execution time of the program was, for most cases, approximately 25 CPU hours using a Sun SparcStation10. If we assume that the Compton scattering distribution is slowly varying over the object, coarser sampling through the input image volume may be appropriate. By sampling over regions equivalent to 4x4 pixels, the execution time of the calculation was reduced by over an order of magnitude to less than 2 hours. Figure 7 shows smoothed profiles through attenuation corrected scatter sinograms calculated by both the fine and the coarsely sampled cases. The two calculated scattered distributions compare well (overall to within 6% in mean number of counts) indicating that little error in the calculation of the scatter contribution is introduced by coarser sampling through the input image. For the finely-sampled simulation, scattered events comprise approximately 38% of the primary photon pairs detected.

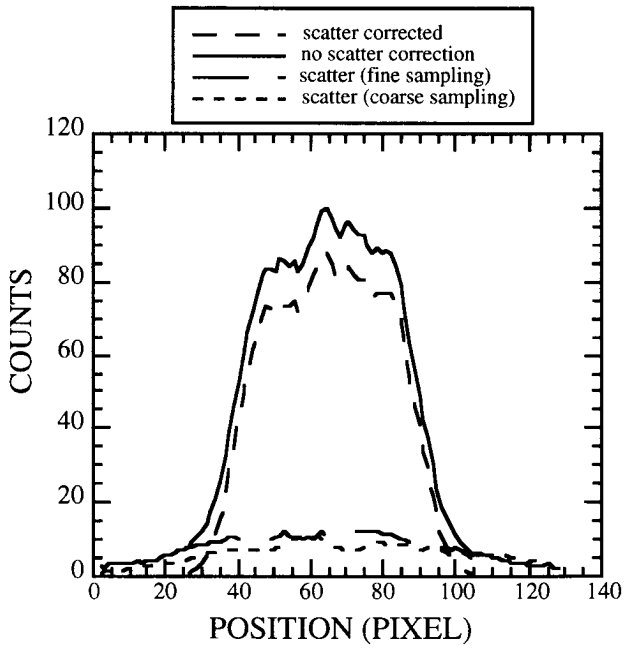

Fig. 7. Profiles through the sinograms of the Monte Carlo calculated uncorrected, corrected and scatter distributions for a 3D human brain study (Legend shown at top). The calculated scatter distributions for the coarse and finely sampled input cases compare well. Computation time for the coarsely sampled case is nearly a factor of 16 times faster than that for fine sampling.

However, since one of the goals in this work is to preserve the accuracy of the scatter calculation, the finer sampling is preferred. We emphasize that this is research grade, non-optimized code that will yield practical execution times with optimization and parallelization. There are no doubt programming improvements to be implemented without compromising accuracy. We are also currently building a workstation based on eight i860 array processors [14] that are expected to improve the computation times by a factor of over 20 over a single Sparc10 CPU. Preliminary data taken show that a single i860 chip was over 3 times faster than a Sparc10 CPU for calculations similiar to those involved in the Monte Carlo code. With eight of such processors running in parallel, the expected computation time of the simulation for the finely (coarsely) sampled case would be < 1 hour (5 minutes).

IV. DISCUSSION

Our results indicate that the Monte Carlo approach to scatter correct fully 3D PET brain images is an important addition to those methods currently used. This method is activity distribution dependent. The program models the statistical emission process in a simulated 3D PET acquisition and calculates the 3D scatter distribution using, as input, an initial 3D reconstruction of the emission data set to be corrected for scatter. The calculated scatter contribution is subtracted from the original data set before a second reconstruction is performed. The calculation makes no assumptions of the shapes of the source or scatter distributions or in the physics of Compton scattering. The scatter component of the total activity was calculated for complex activity distributions represented by the stacked 3D image volumes input. Scatter activity in the empty compartment of the Slot Phantom was reduced to less than 2% after correction; the overall scatter fraction was reduced to less than 1% after correction. Any inefficiency in removing scatter is due to the presence of scatter in the input image; the correction could be applied iteratively to reduce this residual scatter.

At this time the simulation has impractical execution times (~25 hours on a Sparc10). As of yet, no approximating techniques to reduce computation time have been utilized, such as lookup tables. We feel this was the best way to preserve the overall accuracy in the calculation. The slow varying nature of the Compton scattering distribution may warrant coarser sampling through the image volume. Assuming that the distribution does not vary over an effective area of 7x7 mm^2 in the input image volume (4x4 pixels) the execution time of the Monte Carlo was decreased by over an order of magnitude (to < 2 hours) while keeping the overall accuracy of the scatter calculation to within 6%. An alternative is to use the power of vector parallel processing to speed up the finely sampled correction to practical (< 1 hour) execution times without approximations. Further technological advancement in computational speed will improve the situation.

The motivation for developing this Monte Carlo correction to Compton scattering effects in 3D PET is to better quantify whole-body surveys for tumor metastases. The generally poor statistics and large imaging area required puts strict limitations on the types of scatter corrections that are appropriate. Uncompensated scatter causes the greatest difficulty when the subject consists of low contrast objects or has regions of interest with low concentrations of isotope. When studying the chest, the assumption of a constant linear coefficient of attenuation is improper since the lung and heart will attenuate photons differently. A low statistics transmission scan could be used to segment the image from which a proper map of attenuation coefficients would be drawn. This attenuation map would be input to the Monte Carlo and the decisions as to whether or not scatter occurs would be made as before.

As a final note we comment that if proper attenuation coefficients are assigned, the Monte Carlo routine can be used to simultaneously correct 3D acquired data for attenuation as well as scatter. Since nearly all attenuation of 511 keV photons in body tissues is due to Compton scatter, the attenuation coefficient A at any given point could then be approximated by the Monte Carlo simulation as:

$$A = \textit{calculated attenuation coefficient} = \frac{(\textit{calculated number of total photon pairs})}{(\textit{calculated number of scattered photon pairs})},$$

This factor would then be applied to the 3D scatter-corrected data before reconstruction.

V. ACKNOWLEDGMENTS

The authors thank Dr. Simon Cherry, Stefan Siegel and Pranab Banerjee for critical comments and suggestions and technical guidance. This research was funded by NIH Training Grant T32 CA 09092, NIH Grant R01-CA-56655, DOE Grant DE-FC03-87-ER 60615 and the Whitaker Foundation.

VI. REFERENCES

[1] M.E. Phelps *et. al.* An Analysis of Signal Amplification Using Small Detectors in Positron Emission Tomography. *J. Comp. Ass. Tom.*, 6: 551 (1982).

[2] S.R. Cherry, M. Dahlbom and E.J. Hoffman. 3D PET Using a Conventional Multi-slice Tomograph without Septa. *J. Comp. Ass. Tom.*, 15(4): 655 (1991).

[3] D.W. Townsend *et. al.* Fully Three-Dimensional Reconstruction for a PET Camera with Retractable Septa. *IEEE Trans. Med. Im.*, 10(4): 505 (1991).

[4] S. Grootoonk *et. al.* Correction for Scatter Using a Dual Energy Window Technique with a Tomograph Operating without Septa. *IEEE Med. Im. Conf. Rec.*, 3:1569 (1991).

[5] D.L. Bailey. Three-dimensional Acquisition and Reconstruction in Positron Emission Tomography. *Ann. Nucl. Med.*, 6:123 (1992).

[6] L. Shao and J.S. Karp. Cross-Plane Scatter Correction-Point Source De-convolution in PET. *IEEE Trans. Med. Im.*, 10(3): 234 (1991).

[7] S.R. Cherry, S.R. Meikle and E.J. Hoffman. Correction and Characterization of Scattered Events in Three Dimensional PET Using Scanners with Retractable Septa. *J. Nuc. Med.*, 34: 671 (1993).

[8] S.R. Cherry and S.C. Huang. Correction and Characterization of Scatter in 3-D PET. *Presented at the 1994 IEEE Medical Imaging Conference.*

[9] J.M. Ollinger and G.C. Johns. Model-based Scatter Correction for Fully-3D PET. *Conf. Rec. 1993 Meeting on Fully Three-dimensional Image Reconstruction*, p. 111.

[10] J.S. Barney, R. Harrop and C.J. Dykstra. Source Distribution Dependent Scatter Correction for PVI. *IEEE Trans. Nucl. Sci.* NS-38: 719 (1993).

[11] M. Dahlbom *et. al.* A Study of the Possibility of Using Multi-Slice PET Systems for 3D Imaging. *IEEE Trans. Nuc. Sci.* NS-36: 1066 (1989).

[12] S.R. Cherry, M. Dahlbom and E.J. Hoffman. Evaluation of a 3D Reconstruction Algorithm for Multi-slice PET Scanners. *Phys. Med. Biol.*, 37(3): 779 (1992).

[13] S. Siegel and M. Dahlbom. Implementation and Evaluation of a Calculated Attenuation Correction for PET. *IEEE Trans. Nuc. Sci.*, 39: 1117 (1992).

[14] T.M. Guerrero *et. al.* 3D PET Reconstruction Workstation: 1. Design and Construction. *IEEE Conf. Rec.*, 2: 1096 (1993).